JSR Publications

Available Online

J. Sci. Res. **6** (1), 11-27 (2014)

JOURNAL OF SCIENTIFIC RESEARCH

www.banglajol.info/index.php/JSR

New MAX Phase Superconductor Ti_2GeC: A First-principles Study

M. A. Hadi[1*], M. Roknuzzaman[1], F. Parvin[1], S. H. Naqib[1], A. K. M. A. Islam[2] and M. Aftabuzzaman[3]

[1]Department of Physics, Rajshahi University, Rajshahi 6205, Bangladesh

[2]International Islamic University Chittagong, 154/A College Road, Chittagong 4302, Bangladesh

[3]Department of Physics, Pabna University of Science and Technology, Pabna 6600, Bangladesh

Received 14 October 2013, accepted in revised form 19 December 2013

Abstract

This is the first DFT-based first-principles prediction of the detailed optical and thermodynamic properties, including Vickers hardness and Fermi surface of 211 MAX phase Ti_2GeC for which superconductivity (T_c~ 9.5 K) was reported very recently. The calculated structural properties are in excellent agreement with experiments. Our results on elastic parameters indicate a slight elastic anisotropy and brittleness of the compound. The chemical bonding is seen to be a combination of covalent, ionic and metallic nature. The rather stronger covalent bonding is responsible for its high Vickers hardness of 11.6 GPa. The investigated Fermi surface is formed mainly by the low-dispersive bands, which should be responsible for the presence of superconductivity in Ti_2GeC. All the optical properties are evaluated and analyzed for two different polarization directions of incident photon. The temperature and pressure dependence of primitive cell volume, thermal expansion coefficient, specific heats, bulk modulus, and Debye temperature of Ti_2GeC are derived from the quasi-harmonic Debye model with phononic effect and the various implications are discussed in details.

Keywords: First-principles calculation; Vickers hardness; Optical properties; Thermodynamic properties.

doi: http://dx.doi.org/10.3329/jsr.v6i1.16604 J. Sci. Res. **6** (1), 11-27 (2014)

1. Introduction

Very recently, through the electrical resistivity and magnetization measurements, Bortolozo *et al*. have shown that the bulk superconductivity is induced at 9.5 K in Ti_2GeC [1], a compound belonging to the MAX phases. The MAX phases are a class of layered ternary carbides and nitrides, which have the chemical formula: $M_{n+1}AX_n$, where M is an early transition metal, A is an A-group element (comes from Columns 13-16 in the periodic table), X is either C and/or N, and *n* varies from 1 to 3. These ternary compounds

* *Corresponding author*: hadipab@gmail.com

attract more and more attention due to a unique combination of metallic and ceramics properties [2].

To date, among more than 70 synthesized MAX phases [3], bulk superconductivity was discovered for seven systems: Mo_2GaC [4], Nb_2SC [5], Nb_2SnC [6], Nb_2AsC [7], Ti_2InC [8], Nb_2InC [9], and Ti_2InN [10]. Very recently, a superconducting transition at T_C ~ 9.5 K was reported for the eighth MAX phase – Ti_2GeC [1]. Ti_2GeC was first synthesized in 1963 by Jeitschko *et al*. with a = 3.079 Å and c = 12.930 Å [11]. Ti_2GeC as a member of 211 MAX phases has not received adequate attention compared to the other MAX phases. To the best of our knowledge, except structural properties [11-14], no experimental work on other properties has been made for Ti_2GeC. Theoretical studies on structural [15-18], elastic [15, 16, 18], and electronic [15-17, 19, 20] properties of Ti_2GeC were carried out. A theoretical report [18] on some thermodynamic properties such as temperature and pressure dependent linear thermal expansion coefficient as well as pressure dependent bulk modulus and Debye temperature is available. On the other hand, up to now, only optical conductivity [20] of Ti_2GeC is calculated. A complete study on optical as well as thermodynamic properties is absent for Ti_2GeC. Today, knowledge of optical properties of solids is especially important for the design and analysis of new optoelectronic devices [21]. High dielectric materials can be used in the next generation of microelectronic devices in which the reduced dimension requires gate insulators with high dielectric constants [22]. Further, the MAX phases have the potential to be used as a coating on spacecrafts to avoid solar heating [23]. Again, the thermodynamic properties are the basis of solid-state science and industrial applications since they can extend our knowledge on the specific behaviour of materials under high pressure and high temperature environments [24]. Therefore, we are encouraged to investigate the detailed thermodynamic and optical properties of Ti_2GeC for the first time along with the shape of the Fermi surface and Vickers hardness. For justification of the reliability of the present study, we have also revisited the structural, elastic, and electronic properties studied in earlier theoretical works [15-17, 19, 20].

2. Computational details

The first-principles calculations have been performed by employing pseudopotential plane-wave approach based on the density functional theory (DFT) [25] implemented in the CASTEP code [26]. The exchange-correlation potential is evaluated by using the generalized gradient approximation (GGA) with the functional developed by Perdew-Burke-Ernzerhof [27] known as the PBE scheme. Vanderbilt-type ultrasoft pseudopotentials [28] with $3d^2 4s^2$, $4s^2 4p^2$, and $2s^2 2p^2$ as the basis set of the valence electron states for Ti, Ge, and C, respectively, are employed to describe the electron-ion interactions. The energy cutoff of the plane-wave basis set is chosen as 500 eV to determine the number of plane waves in the expansion. For the Brillouin zone integration, the Monkhorst-Pack scheme [29] is used to produce a uniform grid of k-points along the three axes in reciprocal space, and a $12 \times 12 \times 2$ special k-points are taken to achieve

geometry optimization. The Broyden-Fletcher-Goldfarb-Shanno (BFGS) minimization technique [30] is used to search for the ground state of crystal and convergence tolerance is set to energy change below 5.0×10^{-6} eV/atom, force less than 0.01 eV/Å, stress less than 0.02 GPa, and change in atomic displacement less than 5.0×10^{-4} Å. To obtain the smooth Fermi surface, $38 \times 38 \times 8$ *k*-point mesh has been used.

The quasi-harmonic Debye model [31, 32] implemented in the Gibbs program [31] is employed to determine the thermodynamic properties at ambient and elevated temperatures and pressures. In this investigation, we have used energy-volume data calculated from the third-order Birch-Murnahgan equation of state [33] using the zero temperature and zero pressure equilibrium values of energy, volume, and bulk modulus obtained through present DFT calculations.

3. Results and Discussion

3.1. *Structural properties*

Like other MAX phases, Ti_2GeC crystallizes in the hexagonal structure with space group $P6_3/mmc$ (No. 194) and has eight atoms with two formula units in each unit cell (Fig. 1). The calculated values of the lattice parameters and unit cell volume as determined from geometry at zero pressure are listed in Table 1 along with the values obtained in experiments [11-14] and other first-principles calculations [15-18]. Our computed lattice constants *a* and *c* deviate not more than 0.48% of the experimental values, whereas the previous theoretical results deviate by 1.78%. The deviations of unit cell volume calculated in present and previous study from the experimental data are within 0.49% and 3.86%, respectively. It is obvious that our calculated structural properties are very close to the existing experimental values, which shows the reliability of the present first-principles investigations.

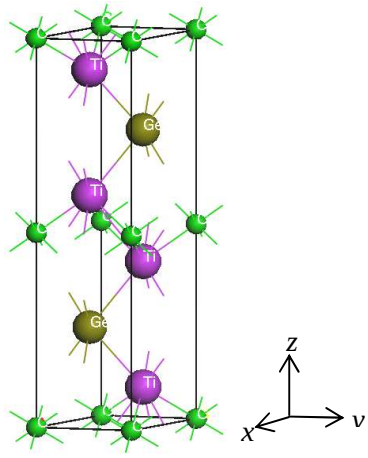

Fig. 1. Crystal structure of Ti_2GeC

Table 1. Calculated lattice parameters (a, c in Å), ratio c/a, internal parameter (z), and cell volume (V_o in Å^3) for superconducting Ti_2GeC in comparison with available data.

a	c	c/a	z	V_o	Ref.
3.079	12.930	4.199	0.0860	106.16[a]	[11] Expt.
3.07	12.93	4.2117	-	105.54[a]	[12] Expt.
3.078	12.934	4.2021	-	106.13	[13] Expt.
3.081	12.929	4.197	0.0953	10 6.29[a]	[14] Expt.
3.0848	12.9609	4.2015	0.0891	106.81	Present
3.0544	12.8914	4.2206	0.0903	104.16[a]	[15]
3.0473	12.7763	4.1927	0.0915	102.75[a]	[16]
3.09	13.04	4.2201	0.0885	107.83[a]	[17]
3.101	13.159	4.2435		109.61	[18]

[a] calculated using published data of respective authors.

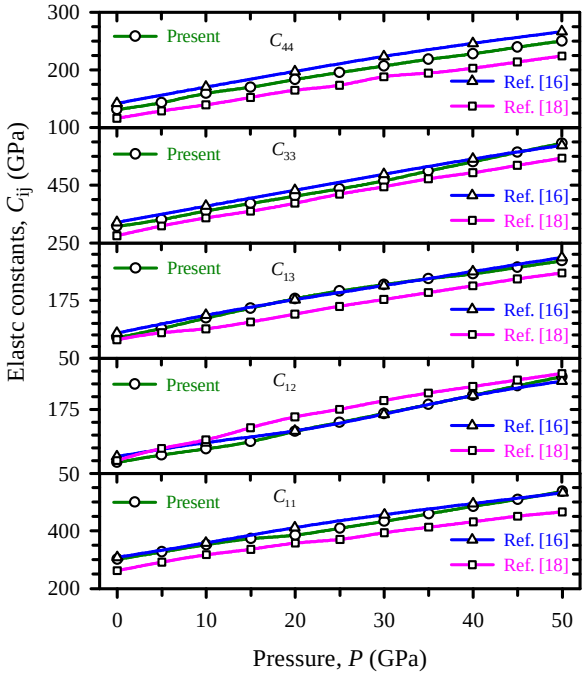

Fig. 2. Pressure dependence of elastic constants C_{ij} of Ti_2GeC

3.2. *Elastic properties*

In Table 2, we have listed the calculated elastic constants along with the available theoretical data for comparison. At present, no experimental data are available. Our results are consistent with the previous reported values [15, 16, 18]. The pressure dependence of the elastic constants C_{ij} is shown in Fig. 2 that reveals the monotonous increase of the five

independent elastic constants C_{ij} with pressure up to 50 GPa. Our calculated C_{13} and C_{33} increase more rapidly with pressure than C_{11}, C_{12}, and C_{44}, which is consistent with the theoretical results obtained by Cui *et al*. [16], whereas according to the values calculated by Fu *et al*. [18], C_{12} and C_{33} vary rapidly with the increase of pressure, followed by C_{11}, C_{13}, and C_{44}.

Table 2. The calculated elastic constants C_{ij} (in GPa) and the shear anisotropic factors A, k_c/k_a of superconducting MAX phase Ti_2GeC compared with other theoretical results.

C_{11}	C_{12}	C_{13}	C_{33}	C_{44}	C_{66}	A	k_c/k_a	Ref.
301	72	94	307	131	115	1.2457	0.87	Present
279	99	95	283	125	90.0	1.3441	1.00	[15]
309.45	83.75	105.09	321.43	142.5	112.85	1.3549	0.85	[16]
280.63	81.43	98.52	294.46	121.5	99.6	1.2500	0.84	[18]

The calculated shear anisotropy factor, defined by $A = 4C_{44}/(C_{11} + C_{33} - 2C_{13})$, implies that Ti_2GeC possesses small anisotropy for the shear planes $\{1\ 0\ \bar{1}\ 0\}$ between the directions $\langle 0\ 1\ \bar{1}\ 1\rangle$ and $\langle 0\ 1\ \bar{1}\ 0\rangle$. This small anisotropy indicates that the in-plane and out-of-plane inter-atomic interactions in Ti_2GeC differ slightly. We have also evaluated another anisotropy parameter defined by the ratio between linear compressibility coefficients along the c and a axis for hexagonal crystal: $k_c/k_a = (C_{11} + C_{12} - 2C_{13})/(C_{33} - C_{13})$. Our result agrees well with other values [16, 18] except for Bouhemadou [15] and reveals that the compressibility along the c axis is slightly less than that along the a axis. This factor also indicates that Ti_2GeC is characterized by a small anisotropy.

We have estimated the bulk modulus B and shear modulus G of polycrystalline aggregates from individual elastic constants, C_{ij} by the well-known Voigt [34] and the Reuss [35] approximations combined with Hill [36] suggestion. We also calculated the Young's modulus Y and Poisson's ratio ν. All these properties are presented in Table 3 together with other results. According to Pugh's criteria [37] and the value of Poisson's ratio [38], Ti_2GeC should behave in a brittle manner.

Table 3. The calculated Bulk moduli (B_R, B_V, B in GPa), shear moduli (G_R, G_V, G in GPa), Young's modulus (Y in GPa), Compressibility (K in GPa^{-1}), G/B, and Poisson's ratio (ν) in comparison with available data.

B_R	B_V	B	G_R	G_V	G	Y	G/B	ν	Ref.
158.48	158.77	158.62	117.63	118.73	118.18	284.0	0.745	0.202	Present
157.60	157.60	157.60	102.30	104.80	103.60	254.9	0.657	0.231	[15]
169.40	169.80	169.60	120.41	122.67	121.54	294.3	0.717	0.211	[16]
156.58	156.96	156.77	105.62	107.00	106.31	260.1	0.678	0.223	[18]

3.3. *Electronic and bonding properties*

The investigated band structure for Ti_2GeC at equilibrium lattice parameters along the high symmetry directions in the first Brillouin zone is shown in Fig. 3a in the energy range from -15 to 5 eV. The band structure of superconducting phase Ti_2GeC reveals 2D-like behaviour with small energy dispersion along the c axis and in the K-H and L-M directions. The Fermi level of Ti_2GeC lies below the valence band maximum near the Γ point as found in literature [15, 16, 19]. The occupied valence bands of Ti_2GeC lie in the energy range from -5.9 eV to Fermi level E_F. Moreover, many valence bands go across the Fermi level and overlap with conduction bands. As a result, there is no band gap at the Fermi level and Ti_2GeC shows metallic behaviour.

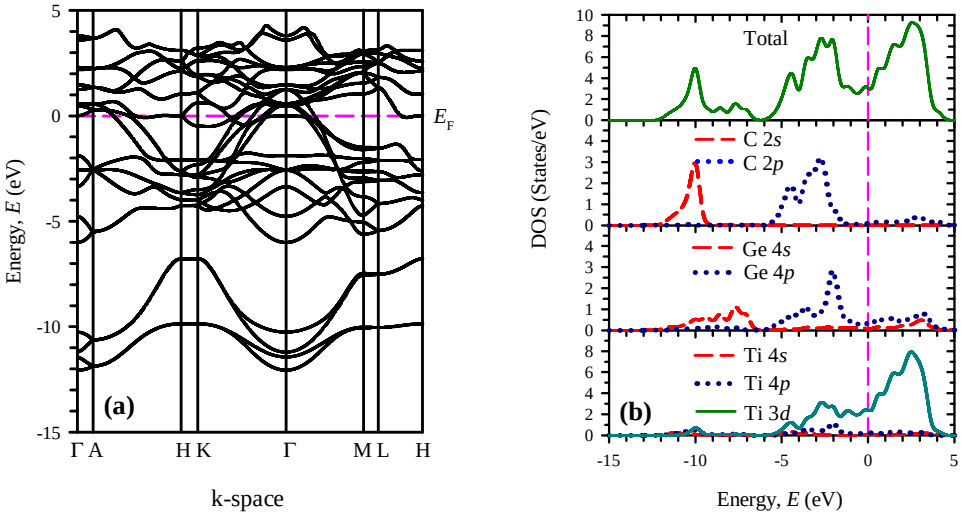

Fig. 3(a). Band structure and (b) total and partial density of states for Ti_2GeC at zero pressure.

The calculated total and partial density of states (DOS) for Ti_2GeC are presented in Fig. 3b. The total DOS at the Fermi level for Ti_2GeC is 3.04 states per unit cell per eV. This value is similar to those found in literature [15-17] and slightly smaller than those obtained in literature [19, 20]. At the Fermi level, the DOS mainly originates from the Ti 3*d* states for this phase. This 3*d* contribution is responsible for the conduction properties of Ti_2GeC. C does not contribute to the DOS at the Fermi level and therefore is not involved in the conduction properties. Ge has a poor contribution at the Fermi level. These results are consistent with previous reports on MAX phases [40]. An intense peak in the total DOS located between – 1.5 and – 5.9 eV below the Fermi level arises from the strong hybridization of Ti 3*d*-C 2*p* states, which plays the role for the covalent Ti-C bonding inside [TiC] blocks in Ti_2GeC. The hybridization of Ti 3*d* and Ge 2*p* states is also visible. Hence, a covalent interaction occurs between [TiC] blocks and Ge sheets. The *p-d* bonding of Ti-C stabilizes the structure of Ti_2GeC while the presence of Ge

changes the Ti-C-Ti-C covalent bond chain into a Ti-C-Ti-Ge bond chain through its reaction with Ti. Also, due to having different electronegativity in different constituent atoms, some ionic character can be expected. Therefore, the bonding nature in Ti_2GeC may be described as a mixture of covalent, ionic, and, due to the *d* resonance in the vicinity of the Fermi level, metallic.

The total and partial density of states in Fig. 3b show that the lowest valence bands from –12.0 to –6.7 eV below the Fermi level are originated by the main contributions of C 2*s*, Ge 4*s*, and Ti 3*d* states with a small mixture of Ti 4*s* and 4*p* states. These valence bands are separated by a narrow forbidden gap (about 0.8 eV) from the higher valence bands, which are located in the energy range from -5.9 eV to E_F. The higher valence bands arise mainly from mixed Ti 3*d*, 4*p*, Ge 4*p* and C 2*p* states. Above the Fermi level, antibonding Ti 3*d* states dominate with less contribution from Ge 4*p* and C 2*p* states.

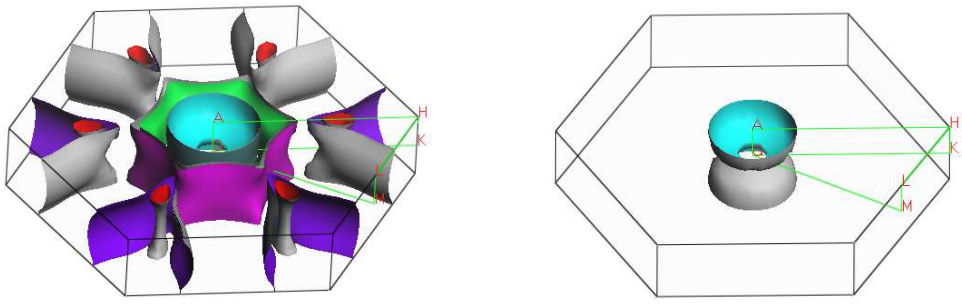

(a) (b)

Fig. 4. (a) Fermi surface of Ti_2GeC and (b) sand-watch like first sheet centered along Γ-A direction.

3.4. *Fermi surface*

The investigated Fermi surface of Ti_2GeC is presented in Fig. 4. The centre of the Fermi surface consists of four hole-like sheets with different topology centered along the Γ-A direction. The first sheet is sand-watch shaped and surrounded by very close cylindrical-like second sheet. The remaining two sheets are cylindrical-like with hexagonal cross-section. These two sheets are nearly closed but apart from the second sheet. There is also additional electron and hole-like sheets along the H-K direction. Fermi surface is formed mainly by the low-dispersive bands, which should be responsible for the superconductivity in the compound.

3.5. *Mulliken bond population and Vickers hardness*

Mulliken bond populations provide a deep understanding about the bonding nature in crystals and the first-key step of calculating the theoretical Vickers hardness. To estimate

accurately the values of Vickers hardness of metallic crystals, the already established empirical formula is as follows [40, 41]:

$$H_V = \left[\prod^{\mu} \left\{ 740\left(P^{\mu} - P^{\mu'}\right)\left(v_b^{\mu}\right)^{-5/3} \right\}^{n^{\mu}} \right]^{1/\Sigma n^{\mu}} , \quad (1)$$

where P^{μ} is the Mulliken bond overlap population of the μ-type bond, $P^{\mu'}$ is the metallic population, v_b^{μ} is the bond volume of μ-type bond, and n^{μ} is the number of μ-type bond.

Table 4 lists the results obtained from the calculations. The Mulliken bond populations may be described as a measure of the degree of overlap of the electron clouds of two bonding atoms in the crystal, and this result indicates that the bond strength increases with overlap population. Its highest and lowest values signify the strength of covalency and ionicity in the chemical bonds, respectively. Accordingly, the Ti-C bonds possess stronger covalent bonding than Ti-Ti bonds in superconducting phase Ti_2GeC. Our calculated Vickers hardness for Ti_2GeC is 11.6 GPa. The measured value of Vickers hardness for Ti_2GeC under a load of 10 kg is 5.5 GPa [42]. The experimental values depend on the purity of the samples. For instance, Ivchenko *et al*. [43, 44] reported experimental Vickers hardness of 21 and 24 GPa for Ti_2AlC and Ti_2AlN, respectively, whereas the respective values measured by Barsoum *et al*. [42] are 5.5 and 3.5 GPa. In spite of this comment, more work, especially theoretical work, is required to better understand this intriguing discrepancy.

Table 4. Calculated Mulliken bond overlap population P^{μ}, bond length d^{μ}, bond volume v_b^{μ} (Å^3) and Vickers hardness H_v^{μ} of μ-type bond, metallic population $P^{\mu'}$, and Vickers hardness H_v of Ti_2GeC.

Bond	d^{μ} (Å)	P^{μ}	$P^{\mu'}$	v_b^{μ} (Å^3)	H_v^{μ} (GPa)	H_v (GPa)
Ti-C	2.1227	1.06	0.0181	5.572	44.03	11.6
Ti-Ti	4.1706	0.58	0.0181	42.261	0.81	

3.6. *Optical properties*

To extract all optical properties, the frequency dependent dielectric function is a key optical quantity, $\varepsilon(\omega) = \varepsilon_1(\omega) + i\varepsilon_2(\omega)$, which keeps up a close relation to the electronic band structure. On the basis of the momentum matrix elements between the occupied and unoccupied electronic states, the imaginary part $\varepsilon_2(\omega)$ of the dielectric function can be expressed as:

$$\varepsilon_2(\omega) = \frac{2e^2\pi}{\Omega\varepsilon_0} \sum_{k,v,c} \left| \left\langle \psi_k^c \left| \hat{u} \cdot \vec{r} \right| \psi_k^v \right\rangle \right|^2 \delta(E_k^c - E_k^v - E) , \quad (2)$$

where ω is the frequency of light, e is the electronic charge, $\hat{u}$ is the vector defining the polarization of the incident electric field, and ψ_k^c and ψ_k^v are the conduction and valence band wave functions at k, respectively. The Kramers-Kronig relations provide the real part of the dielectric function through a transformation from the imaginary part. The remaining optical properties, such as refractive index, absorption spectrum, loss-function, reflectivity and photoconductivity (real part) are derived from $\varepsilon_1(\omega)$ and $\varepsilon_2(\omega)$ [45]. Both inter-band and intra-band transitions contribute to the dielectric function of the metallic compounds. Our calculated band structure ensures that Ti_2GeC behaves as a metallic compound. For this reason, a Drude term [23, 46] with unscreened plasma frequency 3 eV and damping 0.05 eV has been used in the present calculation. Through this effect the low energy part of the spectrum is enhanced significantly. For all calculations, we have used a 0.5 eV Gaussian smearing.

The calculated optical properties of the new superconducting phases Ti_2GeC for phonon energies up to 20 eV for two different polarization directions [100] and [001] are depicted in Fig. 5. Dielectric function is the most general property of a solid, which modifies the incident electromagnetic wave of light. The real and imaginary parts of the dielectric functions of Ti_2GeC are displayed in Figs. 5a and 5b along with the measured values of $TiC_{0.9}$ [47] for comparison. In the range of $\varepsilon_1 < 0$, the real part of the dielectric function goes through zero from below, which reveals the metallic characteristic of Ti_2GeC. In the real part, it is seen that the double peak structure centered at 1.7 eV for TiC is replaced with a sharp peak at around 1.0 eV and 1.5 eV for Ti_2GeC with polarization directions [100] and [001], respectively. In Fig. 5b, the imaginary part of the dielectric function for both directions approaches zero from above, which also indicates that Ti_2GeC is metallic in nature. In $\varepsilon_2(\omega)$, the spectra differ at low energy, due to the change of electronic structure near the Fermi level, caused by the addition of Ge layer in TiC.

In optics, the index of refraction of an optical medium is a dimensionless number that describes how light, or any other radiation, propagates through that medium. The real part of the refractive index of Ti_2GeC is illustrated in Fig. 5c. The static refractive indices of Ti_2GeC for the polarization vectors [100] and [001] are found to have the values 84.56 and 84.58, respectively. The nature of the variation of the refractive index of Ti_2GeC for two different polarization directions with incident light energy is almost same between 6.2 and 20 eV but differs slightly in the low energy region. The extinction coefficient i.e. imaginary part of the refractive index indicates the amount of absorption loss when the electromagnetic wave propagates through the material. The extinction coefficients of Ti_2GeC for two different propagation directions are presented in Fig. 5d. For two different polarization directions, the extinction coefficients of Ti_2GeC show the same qualitative features in entire energy range except 1-7 eV regions.

The absorption coefficient provides information regarding optimum solar energy conversion efficiency and it indicates how far light of a specific energy (wavelength) can penetrate into the material before being absorbed. Fig. 5e shows the absorption spectra of Ti_2GeC for both polarization directions, which begin at zero photon energy due to its

metallic nature. The absorption spectra for two polarization directions arise sharply below 5.5 eV and the highest peaks for polarization directions [100] and [001] appear at 6.28 and 5.99 eV, respectively and then decrease drastically up to 13.7 eV. Again, the absorption spectra show a sharp dip from 13.7 to 14.6 eV. The highest peak is associated with the transition from Ge/C *p* to Ti *d* states.

The energy loss function of a material is a key parameter in the dielectric formalism used to describe the optical spectra and the excitations produced by swift charges in solid. The energy loss function of Ti_2GeC for both polarization directions is shown in Fig. 5f. The frequency associated with the highest peak of energy loss spectrum is known as the bulk plasma frequency ω_p of the material, which appears at $\varepsilon_2 < 1$ and $\varepsilon_1 = 0$ [46, 48]. From the energy loss spectra, it is seen that the plasma frequency of Ti_2GeC is equal to 14.5 eV, which means that the superconducting phase Ti_2GeC will be transparent if the incident light has frequency greater than 14.5 eV and will change from a metallic to a dielectric response.

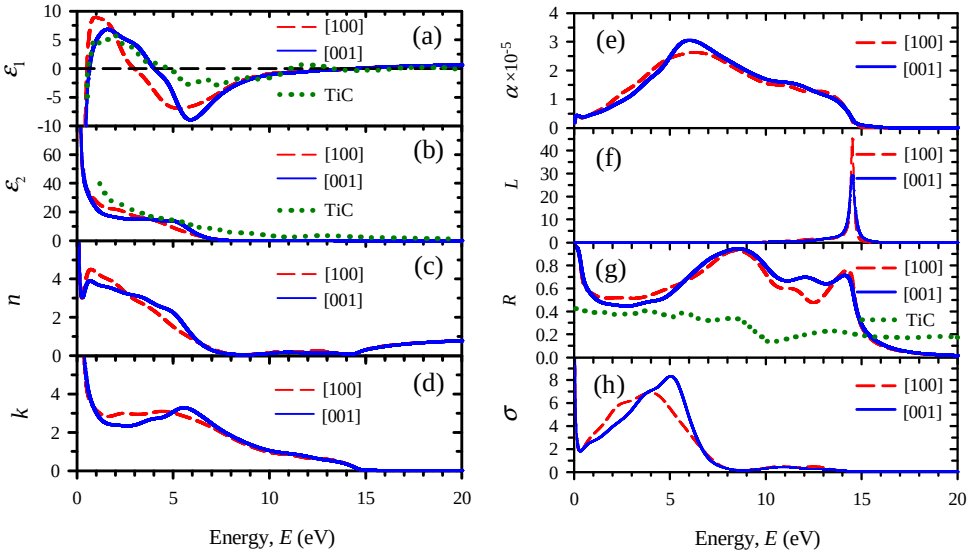

Fig. 5. (a) Real and (b) imaginary part of dielectric function, (c) real and (d) imaginary part of refractive index, (e) absorption coefficients, (f) loss function, (g) reflectivity, and (h) real part of photoconductivity of Ti_2GeC in both [100] and [001] directions. Experimental data shown for TiC are from ref. [47].

Reflectivity is the ratio of the energy of a wave reflected from a surface to the energy possessed by the wave striking the surface. The reflectivity spectra of Ti_2GeC as a function of incident light energy are presented in Fig. 5g. For comparison, the measured spectra of $TiC_{0.97}$ [47] are shown in the plot. The reflectance of $TiC_{0.97}$ is roughly constant in the energy region from 0 to 8.5 eV. A gradual decrease starts at 8.5 eV and ends at 10.4

eV. Again, the reflectivity of $TiC_{0.97}$ increases to reach another almost constant value. By addition of Ge to TiC, the reflectivity increases rapidly in the moderate-infrared region as well as in the ultraviolet region of the energy range 4.6 – 8.5 eV and decreases drastically from 14.2 to 15.1 eV. In the visible light region (energy range ~1.8-3.1 eV), it is observed that for both polarization orientations there is no significant change in reflectivity spectra for Ti_2GeC and the amount of reflectivity is always above 44%. Due to this nearly constant reflectivity in the visible light region the superconducting phase Ti_2GeC should appear as metallic gray. Further, the reflectivity spectra for the two different polarization directions increase expeditiously to reach maximum value of ~ 0.93 – 0.95 in the ultraviolet region (between 8.46 and 8.53 eV). According to Li *et al*. [23], the MAX phase compound will be capable of reducing solar heating if it has reflectivity ~ 44% in the visible light region. Therefore, we may conclude that Ti_2GeC is also a candidate material for coating to reduce solar heating.

Photoconductivity is an optoelectrical phenomenon in which a material increases its electrical conductivity due to the absorption of electromagnetic radiation. The photoconductivity may be expected to be a good measure of optical conductivity. Absolutely, it was illustrated in $Nd_2CuO_{4-\delta}$ [49] by synchronous measurements of both the optical and photoconductivity. The real part of the photoconductivity of Ti_2GeC for two different polarization directions is shown in Fig. 5h. It is seen that photoconductivity occurs at zero photon energy due to the overlapping of the valence and conduction bands at the Fermi level. Therefore, photocurrent can be generated within a wide range of photon energies. The photoconductivity shows a sharp dip from 0 to 0.3 eV and then inclines upward to reach maximum value of ~ 6.9 – 8.3 for polarization directions [100] and [001] in the ultraviolet region (between ~ 4.0 and 5.0 eV). Therefore, Ti_2GeC will be highly electrically conductive when the incident radiation has energy within the range of ~ 4.0 to 5.0 eV. The enhancement of electrical conductivity due to absorption of electromagnetic radiation of photon energy within 8.5 to 16.2 eV is so small. There is no photoconductivity when the photon energy is higher than 16.2 eV.

3.7. *Thermodynamic properties*

The thermodynamic properties are evaluated in the temperature range from 0 to 1200 K, where the quasi-harmonic Debye model remains fully valid. The pressure effect is studied in the 0-50 GPa range. The temperature and pressure dependence of primitive cell volume V of Ti_2GeC is shown in Figs. 6a and 6b. The volume increases almost linearly with the increase of temperature at constant pressure. For a given temperature, the primitive cell volume decreases with increasing pressure. The pressure dependence of experimental [13] and equilibrium theoretical [18] primitive cell volumes are also shown in Fig. 6b. Our results are in reasonable agreement with experiment within the pressure range from 0 to 12 GPa, whereas the theoretical values [18] differ from both present and experimental results in entire pressure range. At P = 0 GPa and T = 0 K, the primitive cell volume is 53.41 $Å^3$.

In Fig. 7, we have represented the variations of the volume thermal expansion coefficient of Ti_2GeC as a function of temperature and pressure. The thermal expansion coefficient is thought to be described as the alteration in a frequency of the crystal lattice vibration based on the lattice's increase or decrease in volume as the temperature changes. It is observed that, at a given pressure, the volume thermal expansion coefficient increases sharply with increasing temperature up to 300 K. When the temperature exceeds 300 K, the volume thermal expansion coefficient progressively approaches a linear increase with increasing temperature and the tendency of increment becomes very moderate, which means that the temperature dependence of volume thermal expansion coefficient is very small at high temperature. As seen in Fig. 7a, for temperature above 300 K and pressure P = 50 GPa, Ti_2GeC has a nearly constant volume thermal expansion coefficient α_V = 1.75×10^{-5} K^{-1}. At constant temperature, the volume thermal expansion coefficient decreases rapidly with increasing pressure (Fig. 7b). At 300 K and zero pressure, the volume thermal expansion coefficient is 3.155×10^{-5} K^{-1}.

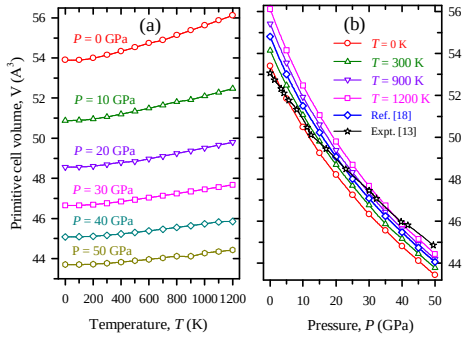

Fig. 6. (a) Temperature and (b) pressure dependence of primitive cell volume of Ti_2GeC.

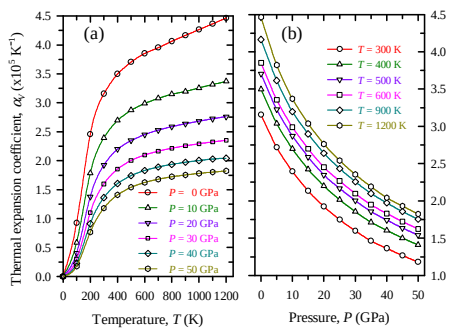

Fig. 7. (a) Temperature and (b) pressure dependence of volume thermal expansion coefficient of Ti_2GeC.

The constant-volume specific heat C_V and constant-pressure specific heat C_P of Ti_2GeC are calculated and shown in Fig. 8. We observed that both specific heats increase with increasing temperature. These results indicate that phonon thermal softening occurs when the temperature is raised. In the low-temperature limit, C_V of Ti_2GeC exhibits the Debye T^3 power-law behavior, and from 0 to about 600 K, C_V increases exponentially. At intermediate temperature, the dependence of C_V is governed by the details of vibrations of atoms and then at high temperature the anharmonic effect on specific heat is restrained. As a result, C_V comes to be close to the classical asymptotic limit of $C_V = 3nNk_B = 99.8$ J/mol K. This result implies that the interactions between ions in Ti_2GeC have great effect on specific heat particularly at low temperatures. The values of C_P for Ti_2GeC are slightly larger than the C_V, which can be explained by the relation: $C_P - C_V = \alpha_V^2(T)BVT$, where α_V, B, V, and T are the volume thermal expansion coefficient, bulk modulus, volume, and absolute temperature, respectively. At high temperatures, the C_V inclines to a nearly

constant value while the C_P increases very slowly with the temperature. As seen in Fig. 8, it is clear that temperature and pressure have opposite influences on the specific heat and the effect of temperature on specific heat is more pronounced than that due to pressure.

We evaluated the electronic contribution to the specific heat through the Sommerfeld constant γ within the free electron model: $\gamma = (1/3)\pi^2 k_B^2 N(E_F)$. Using the calculated DOS, $N(E_F)$ at the Fermi level we obtained γ = 3.57 mJ/mol-K^2 for Ti_2GeC, whereas Lofland *et al*. [7] extracted this value of 4.8 mJ/mol-K^2 by fitting the measured specific heat at low temperature to $C_P = \gamma T + \beta T^3$. We can also determine the electron-phonon coupling constant, λ using the McMillan's formula [50]. Taking the known T_C, and calculated Debye temperature θ_D with the Coulomb pseudopotential μ^* = 0.1, the estimated λ is 0.56, which indicates that Ti_2GeC is moderately coupled superconductor. For comparison, Lofland *et al*. [7] have determined λ for Ti_2GeC from heat capacity and resistivity, yielding values of 0.14 and 0.48, respectively.

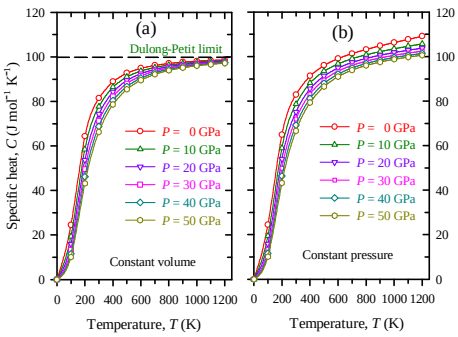

Fig. 8. Temperature dependence of specific heat of Ti_2GeC (a) at constant volume, and (b) at constant pressure.

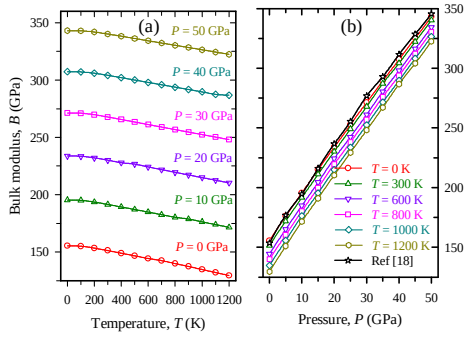

Fig. 9. (a) Temperature and (b) pressure dependence of the bulk modulus of Ti_2GeC.

The dependence of the isothermal bulk modulus of Ti_2GeC on temperature and pressure is shown in Fig. 9. The isothermal bulk modulus provides information about the nature of chemical bonding in crystal and makes it possible to evaluate the Debye temperature, the difference between the heat capacities at constant pressure and volume, and other thermal parameters. It is seen that in Fig. 9a, the bulk modulus is fairly a constant between temperature 0 and 100 K at a given pressure and when temperature exceeds 100 K, it starts to decrease linearly with increasing temperature. When the applied pressure changes from 0 to 50 GPa, the bulk modulus increases by 132% and 149% at temperatures of 600 and 1200 K, respectively. Fig. 9b shows that the bulk modulus of Ti_2GeC increases linearly with the increase of pressure at constant temperature, which is consistent with the results obtained by Fu *et al*. [18]. The effects of temperature on the bulk modulus at different pressures are almost same. At zero pressure and 300 K temperature, the bulk modulus is equal to 151.24 GPa.

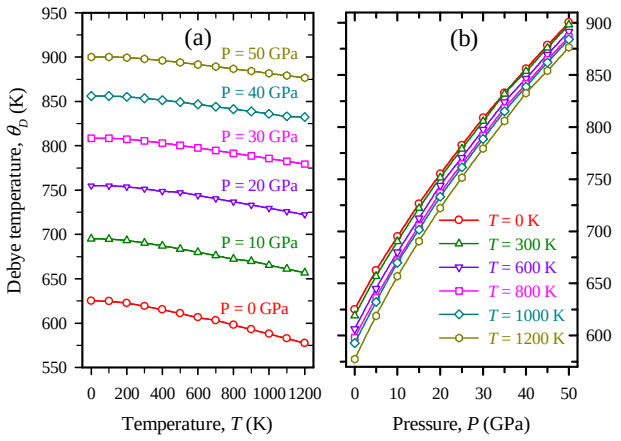

Fig. 10. (a) Temperature and (b) pressure dependence of the Debye temperature of Ti_2GeC

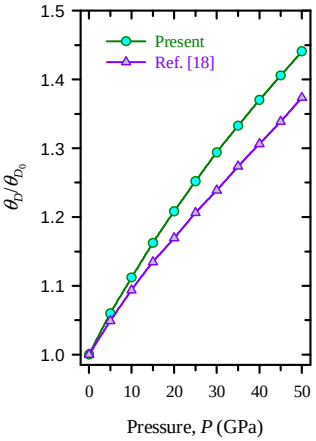

Fig. 11. Normalized Debye temperature of Ti_2GeC as a function of pressure.

The Debye temperature as a function of temperature and pressure is displayed in Fig. 10. We observe that at constant pressure, the Debye temperature θ_D remains unchanged from 0 to 100 K and then decreases linearly with increasing temperature as shown in Fig. 10a. Fig. 10b shows that the Debye temperature increases non-linearly with the increase of applied pressure at constant temperature. The variation of θ_D with pressure and temperature reflects the fact that the thermal vibration frequency of atoms in Ti_2GeC changes with pressure and temperature. At temperatures of 600 and 1200 K, the Debye temperature increases by 47% and 52% if the external pressure changes from 0 to 50 GPa. Fu *et al*. [18] presented their pressure dependence Debye temperature in normalized form with which we have compared our results in Fig. 11.

4. Conclusions

First-principles calculations based on density functional theory have been carried out to investigate the structural stability, elastic properties, electronic structure, Fermi surface, theoretical hardness, optical functions and thermodynamic properties of the newly discovered 9.5 K superconductor Ti_2GeC. The evaluated structural parameters at zero pressure are in excellent agreement with the available experimental data. The calculated elastic parameters allow us to conclude that the superconducting phase Ti_2GeC is mechanically stable compound. In addition, Ti_2GeC is characterized as brittle material and shows a slight elastic anisotropy.

The electronic structure of Ti_2GeC reveals that it is a metal and exhibits covalent nature. Moreover, the Ti-C bonds possessed stronger covalent bonding than the Ti-Ti bonds. The strong covalent bonding in Ti_2GeC is responsible for its high Vickers hardness. At around the Fermi level, the DOS mainly originates from the Ti 3*d* states. The

Ti 3*d*-C 2*p* hybridization is the driving force in the structure and the presence of Ge changes the Ti-C-Ti-C covalent bond chain into a Ti-C-Ti-Ge bond chain, forming a layered structure. The Fermi surface is formed mainly by the low-dispersive bands, which should be responsible for the presence of superconductivity in Ti_2GeC. The optical properties such as dielectric function, refractive index, absorption spectrum, energy-loss function, reflectivity, and photoconductivity are determined and analyzed in detail. The optical properties such as refractive index, reflectivity, and photoconductivity are found to be polarization dependent. The reflectivity spectra imply that Ti_2GeC is a potential candidate material for coating to reduce solar heating. Finally, the temperature and pressure dependence of primitive cell volume, volume thermal expansion coefficient, bulk modulus, Debye temperature, and specific heats are investigated successfully using the quasi-harmonic Debye model and the results are discussed. The increase of specific heats with temperature indicates that phonon thermal softening occurs when the temperature increases. The estimated electron-phonon coupling constant signifies that Ti_2GeC is a moderately coupled superconductor. The present study provides us with clear indications of small anisotropy in the elastic and optical properties of the newly discovered superconducting phase Ti_2GeC.

References

1. A. D. Bortolozo, O. H. Sant'Anna, C. A. M. dos Santos, and A. J. S. Machado, Materials Science-Poland **30**, 92 (2012). http://dx.doi.org/10.2478/s13536-012-0013-4
2. M. W. Barsoum, Prog. Solid State Chem. **28**, 201 (2000). http://dx.doi.org/10.1016/S0079-6786(00)00006-6
3. J. Wang and Y. Zhou, Annu. Rev. Mater. Res. **39**, 415 (2009). http://dx.doi.org/10.1146/annurev-matsci-082908-145340
4. L. E. Toth, J. Less Common Met. **13**, 129 (1967). http://dx.doi.org/10.1016/0022-5088(67)90055-0
5. K. Sakamaki, H. Wada, H. Nozaki, Y. Onuki, and M. Kawai, Solid State Commun. **112**, 323 (1999). http://dx.doi.org/10.1016/S0038-1098(99)00359-2
6. A. D. Bortolozo, O. H. Sant'Anna, M. S. da Luz, C. A. M. dos Santos, A. S. Pereira, K. S. Trentin, and A. J. S. Machado, Solid State Commun. **139**, 57 (2006). http://dx.doi.org/10.1016/j.ssc.2006.05.006
7. S. E. Lofland, J. D. Hettinger, T. Meehan, A. Bryan, P. Finkel, S. Gupta, M. W. Barsoum, and G. Hug, Phys. Rev**. B 74**, 174501 (2006). http://dx.doi.org/10.1103/PhysRevB.74.174501
8. A. D. Bortolozo, J. Fisk, O. H. Sant'Anna, C. A. M. dos Santos, and A. J. S. Machado, Solid State Commun. **144**, 419 (2007). http://dx.doi.org/10.1016/j.ssc.2007.09.028
9. A. D. Bortolozo, O. H. Sant'Anna, C. A. M. dos Santos, and A. J. S. Machado, Physica **C 469**, 256 (2009). http://dx.doi.org/10.1016/j.physc.2009.02.005
10. A. D. Bortolozo, G. Serrano, A. Serquis, D. Rodrigues Jr., C. A. M. dos Santos, Z. Fisk, and A. J. S. Machado, Solid State Commun. **150**, 1364 (2010). http://dx.doi.org/10.1016/j.ssc.2010.04.036
11. W. Jeitschko, H. Nowotny, and F. Benesovsky, Monatsch. Chem. **94**, 1201 (1963). http://dx.doi.org/10.1007/BF00905711
12. M. W. Barsoum, Physical Properties of the MAX phases Encyclopedia of Materials: Science and Technology (Amsterdam, Elsevier, 2004). PMCid:PMC2568667
13. N. A. Phatak, S. K. Sexena, Y. W. Fei, and J. Z. Hu, J. Alloys Compd. **474**, 174 (2009). http://dx.doi.org/10.1016/j.jallcom.2008.06.073

14. M. Y. Gamarnik and M. W. Barsoum, J. Matter. Sci. **34**, 169 (1999). http://dx.doi.org/10.1023/A:1004415018691
15. A. Bouhemadou, Appl. Phys. **A 96**, 959 (2009). http://dx.doi.org/10.1007/s00339-009-5106-5
16. S. Cui, W. Feng, H. Hu, Z. Lv, G. Zhang, and Z. Gong, Solid State Commun. **151**, 491 (2011). http://dx.doi.org/10.1016/j.ssc.2010.12.024
17. G. Hug, Phys. Rev. **B 74**, 184113 (2006). http://dx.doi.org/10.1103/PhysRevB.74.184113
18. H. Fu, W. Liu, Y. Ma, and T. Gao, J. Alloys Compd. **506**, 22 (2010). http://dx.doi.org/10.1016/j.jallcom.2010.06.186
19. Y. C. Zhou, H. Y. Dong, X. H. Wang, and S. Q. Chen, J. Phys.: Condens. Matter **12**, 9617 (2000). http://dx.doi.org/10.1088/0953-8984/12/46/309
20. Y. Mo, P. Rulis, and W. Y. Ching, Phys. Rev. **B 86**, 165122 (2012). http://dx.doi.org/10.1103/PhysRevB.86.165122
21. A. H. Reshak, Z. Charifi, and H. Baaziz, J. Phys.: Condens. Matter **20**, 325207 (2008). http://dx.doi.org/10.1088/0953-8984/20/32/325207
22. M. Xu, S. Wang, G. Yin, J. Li, Y. Zheng, L. Chen, and Y. Jia, Appl. Phys. Lett. **89**, 151908 (2006). http://dx.doi.org/10.1063/1.2360937
23. S. Li, R. Ahuja, M. W. Barsoum, P. Jena, and B. Johansson, Appl. Phys. Lett. **92**, 221907 (2008). http://dx.doi.org/10.1063/1.2938862
24. Y. L. Du, Z. M. Sun, H. Hashimoto, and W. B. Tian, Mater. Trans. **50**, 2173 (2009). http://dx.doi.org/10.2320/matertrans.MAW200903
25. W. Kohn and L. Sham, J Phys. Rev. **140**, A1133 (1965). http://dx.doi.org/10.1103/PhysRev.140.A1133
26. S. J. Clark, M. D. Segall, C. J. Pickard, P. J. Hasnip, M. I. J. Probert, K. Refson, and M. C. Payne, Zeitschrift für Kristallographie **220**, 567 (2005). http://dx.doi.org/10.1524/zkri.220.5.567.65075
27. J. P. Perdew, K. Burke, and M. Ernzerhof, Phys. Rev. Lett. **77**, 3865 (1996). http://dx.doi.org/10.1103/PhysRevLett.77.3865 PMid:10062328
28. J. A. White and D. M. Bird, Phys. Rev. **B 50**, 4954 (1994). http://dx.doi.org/10.1103/PhysRevB.50.4954
29. H. J. Monkhorst and J. D. Pack, Phys. Rev. **B 13**, 5188 (1976). http://dx.doi.org/10.1103/PhysRevB.13.5188
30. T. H. Fischer and J. Almlof, J. Phys. Chem. **96**, 9768 (1992). http://dx.doi.org/10.1021/j100203a036
31. M. A. Blanco, E. Francisco, and V. Luaña, Comput. Phys. Commu. **158**, 57 (2004). http://dx.doi.org/10.1016/j.comphy.2003.12.001
32. M. A. Hadi, M. S. Ali, S. H. Naqib, and A. K. M. A. Islam, Int. J. Comp. Mat. Sci. Eng. **2**, 1350007 (2013). http://dx.doi.org/10.1142/S2047684113500073
33. F. Birch, J. Geophys. Res.: Solid Earth **83**, 1257 (1978). http://dx.doi.org/10.1029/JB083iB03p01257
34. W. Voigt, Lehrbuch der Kristallphysik (Taubner, Leipzig, 1928).
35. A. Z. Reuss, Angew. Math. Mech. **9**, 49 (1929). http://dx.doi.org/10.1002/zamm.19290090104
36. R. Hill, Proc. Phys. Soc. **A 65**, 349 (1952). http://dx.doi.org/10.1088/0370-1298/65/5/307
37. S. F. Pugh, Philos. Mag. **45**, 823 (1954).
38. J. Haines, J. M. Léger, and G. Bocquillon, Annu. Rev. Mater. Res. **31**, 1 (2001). http://dx.doi.org/10.1146/annurev.matsci.31.1.1
39. G. Hug and E. Fries, Phys. Rev**. B 65**, 113104 (2002). http://dx.doi.org/10.1103/PhysRevB.65.113104
40. F. M. Gao, Phys. Rev. **B 73**, 132104 (2006). http://dx.doi.org/10.1103/PhysRevB.73.132104
41. H. Y. Gou, L. Hou, J. W. Zhang, and F. M. Gao, Appl. Phys. Lett. **92**, 241901 (2008). http://dx.doi.org/10.1063/1.2938031
42. M. W. Barsoum, D. Brodkin, and T. El-Raghy, Scr. Mater. **36**, 535 (1997). http://dx.doi.org/10.1016/S1359-6462(96)00418-6

43. V. I. Ivchenko, M. I. Lesnaya, V. F. Nemchenko, and T. Y. Kosolapova, Porosh. Metall. **160**, 60 (1976).
44. V. I. Ivchenko, M. I. Lesnaya, V. F. Nemchenko, and T. Y. Kosolapova. Porosh. Metall. **161**, 45 (1976).
45. S. Shaha, T. P. Sinha, and A. Mookarjee, Phys. Rev. **B 62**, 8828 (2000). http://dx.doi.org/10.1103/PhysRevB.62.8828
46. R. Saniz, L. H. Ye, T. Shishidou, and A. Freeman, J Phys. Rev. **B 74**, 014209 (2006). http://dx.doi.org/10.1103/PhysRevB.74.014209
47. D. W. Lynch, C. G. Olson, D. J. Peterman, and J. H. Weaver, Phys. Rev. **B 22**, 3991 (1980). http://dx.doi.org/10.1103/PhysRevB.22.3991
48. J. S. de Almeida and R. Ahuja, Phys. Rev. **B 73**, 165102 (2006). http://dx.doi.org/10.1103/PhysRevB.73.165102
49. G. Yu, C. H. Lee, A. J. Heeger, and S. W. Cheong, Physica **C 203**, 419 (1992). http://dx.doi.org/10.1016/0921-4534(92)90051-D
50. W. L. McMillan, Phys. Rev. **167**, 331 (1968). http://dx.doi.org/10.1103/PhysRev.167.331